electronics

MDPI

Article

Analysis of Magnetotherapy Device-Induced Fields Using Cylindrical Human Body Model

Mario Cvetković *,† and Bruno Sučić †

Faculty of Electrical Engineering, Mechanical Engineering and Naval Architecture, University of Split, 21000 Split, Croatia; bruno.sucic.00@fesb.hr

* Correspondence: mcvetkov@fesb.hr

† These authors contributed equally to this work.

Abstract: This paper deals with the analysis of induced current density and the induced electric field in the body of a human exposed to the magnetic field of a magnetotherapy device. As the displacement currents at extremely low frequencies can be neglected, the biological tissues can thus be considered a weakly conducting medium, facilitating the use of a quasi-static eddy current approximation. The formulation is based on the surface integral equation for the unknown surface charges, whose numerical solution is obtained using the method of moments technique. A simplified model of the human body is utilized to examine various scenarios during the magnetotherapy procedure. The numerical results for the induced current density and the induced electric field are obtained using the proposed model. The analyses of various stimulating coil parameters, human body model parameters, and a displacement of the magnetotherapy coil were carried out to assess their effects on the induced current density. The results suggest that selection of the stimulating coil should be matched based on the size of the human body, but also that the position and orientation of the coil with respect to the body surface will result in different distributions of the induced fields. The results of this study could be useful for medical professionals by showing the importance of various magnetotherapy coil parameters for preparation of various treatment scenarios.

Keywords: magnetotherapy; integral equation formulation; induced current density; induced electric field; biomedical application

Citation: Cvetković, M.; Sučić, B. Analysis of Magnetotherapy Device-Induced Fields Using Cylindrical Human Body Model. *Electronics* **2024**, *13*, 849. https://doi.org/10.3390/electronics13050849

Academic Editors: Ilaria Sergi and Teodoro Montanaro

Received: 24 January 2024
Revised: 16 February 2024
Accepted: 19 February 2024
Published: 23 February 2024

1. Introduction

Magnetotherapy is a non-invasive form of medical treatment used to relieve joint or muscular pain and decrease stress. It represents a complementary approach utilized in physiotherapy and rehabilitation of locomotive organs in humans, as well as in veterinary medicine. The technique, in its most frequently used form, is based on the use of extremely low-frequency (ELF) magnetic fields generated by solenoidal coils of various sizes administered over a patient's extremities, neck, or back.

The beginning of modern magnetotherapy is associated with the 1950s, initially starting in Japan and later moving to Europe and the former Soviet Union [1]. Later, during the 1970s, it became a new modality in treating delayed bone fractures [2], subsequently resulting in US Food and Drug Administration approval. Initially, a very specific ELF biphasic signal was used, while a decade later an approach based on the use of a pulsed electromagnetic field (pulsed EMF or PEMF) with a high-frequency was approved for the treatment of superficial soft tissue pain and edema. Compared to time varying EMFs such as those used in PEMF it should be emphasized that the use of static magnets in both reducing pain and altering physiological responses is associated with questionable therapeutic benefits as research studies do not provide conclusive support [3,4].

The historical review of the therapeutic use of static electric and magnetic fields and their current acceptance as alternative and complementary therapies can be found in [5].

Despite of the persisting interest in these medical modalities, the medical establishment is still unconvinced due to the lack of unambiguous proof. The use of a static magnetic field as a form of therapy has been considered in treatments including, but not limited to, chronic pelvic pain [6], carpal tunnel syndrome pain [7], and inflammation due to rheumatoid arthritis [8]. There are many available magnetic devices including bracelets, bands, insoles, braces, pillows, and mattresses that are often marketed as having medical benefits; however, there are no consistent studies showing their therapeutic benefits [9].

Another form of magnetotherapy is PEMF, which has many possible applications. For example, the study in [10] assessed the efficacy of low-frequency PEMF therapy in patients with knee osteoarthritis, concluding that a statistically significant benefit in terms of pain reduction was demonstrated. On the other hand, the sono-electro-magnetic treatment of chronic pelvic pain syndrome did not find a significant improvement compared to the placebo-controlled group, as shown in [11]. Another study [12] examined the effectiveness of magnetotherapy for decreasing chronic low back pain and did not find a statistically significant improvement when compared to control subjects exposed to a non-functioning placebo device. One recent review [13] analyzed the use of PEMF even in non-invasive cancer treatment and concluded that further studies are necessary to establish the efficiency in a clinical environment. Finally, a meta analysis in [14] considered the efficacy of the magnetotherapy approach in the rehabilitation field and concluded that electromagnetic field therapy could alleviate pain and improve function in patients with various forms of musculoskeletal pain.

The applied fields used in ELF magnetotherapy are generally of a sinusoidal waveform with frequencies ranging between 1 Hz and 300 Hz, with a typical frequency of 100 Hz, but there are also high-frequency pain treatment modalities such as non-invasive transcranial magnetic stimulation (TMS) [15] or invasive spinal cord stimulation (SCS) [16], which operate at 10 kHz. The maximum magnetic flux density achieved using a typical magnetotherapy coil is generally between 1 mT and 10 mT.

The exposure of humans to ELF magnetic fields generated by magnetotherapy devices has been analyzed in a number of papers including [17–21]. The study in [17] is based on the analytical approach featuring the disk model of the human body, while most often the numerical approach is based on the use of the finite-difference time-domain method [18,19]. In many numerical analyses, the main focus when calculating the induced eddy current distribution is restricted to a particular body part, such as a knee joint [18,19,21] or a forearm [22]. The full human body model exposure during the magnetotherapy procedure is used to a lesser extent, as evidenced from the available literature [17].

This paper is on the analysis of magnetotherapy device-induced fields in a simplified human body model based on the surface integral equation approach featuring the method of moments technique. This work is an extension of our previous conference paper [23] where our simplified body model was introduced. Compared to [23], additional calculations were carried out to determine the effects of different model parameters on the induced current density distribution. Also, we have extended the analysis to assess the effects of the coil positioning on the induced current density.

This paper is organized as follows: After the current Section 1, Section 2 will provide an overview of the mathematical background, including the formulation based on the quasi-static eddy current approximation for a biological body and its derivation using the boundary conditions for the induced current density. Then, the surface integral equation for the unknown surface charges solved by numerical approach are also discussed. In Section 3, the simplified human body model is introduced, whose validation is carried out by comparing the numerical results with the analytical approach. Section 4 discusses the numerical results for the induced current density and the induced electric field, due to a magnetotherapy procedure, obtained via our proposed model. The analysis of stimulating coil parameters, human body model parameters, and the position of magnetotherapy coil are also discussed in this section. Section 5 provides the concluding remarks. The analytical expression for the induced current density is derived in Appendix A.

2. Mathematical Details

2.1. Problem Formulation

The human body tissues can be considered as weakly conducting, facilitating the use of a quasi-static eddy current approximation. Consider a biological body, represented by the region of electrical conductivity σ_1, enclosed with the boundary surface S, as depicted in Figure 1.

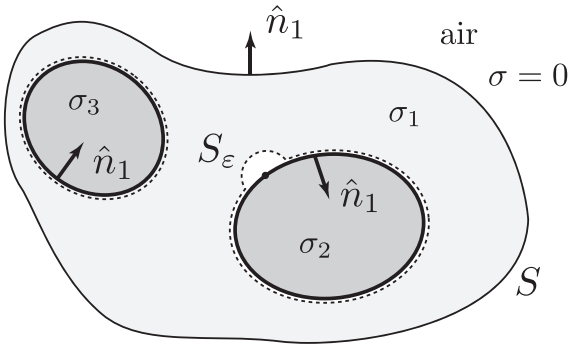

Figure 1. Weakly conducting biological media with conductivity σ_1.

The body is surrounded by an air medium (σ = 0), but it can also be in contact with regions with different values of conductivity, e.q. σ_2 and σ_3.

The differential form of Ohm's law can be used to relate the induced eddy current density with the induced electric field in biological tissue:

$$\vec{J} = \sigma \vec{E} \tag{1}$$

where σ represents the electrical conductivity of tissue.

The normal component of $\vec{J}$ is continuous across interfaces between regions with different parameters. The boundary conditions on the surface S can thus be written as:

$$\sigma_{int} \hat{n}_1 \cdot \vec{E}_{int}(\vec{r}) = \sigma_{ext} \hat{n}_1 \cdot \vec{E}_{ext}(\vec{r}) \tag{2}$$

where $\sigma_{int} = \sigma_1$ is the conductivity of biological media, and σ_{ext} is the conductivity of external medium, σ_2, σ_3, or $\sigma_{air} = 0$. $\vec{E}_{int} = \vec{E}_1$ denotes the electric field in biological media, while $\vec{E}_{ext}$ is the electric field in external regions. The boundary condition on the interface between body and air is thus:

$$\sigma_1 \hat{n}_1 \cdot \vec{E}_1(\vec{r}) = 0 \tag{3}$$

with $\hat{n}_1$ unit as the normal vector.

For time harmonic fields, the electric field can be expressed as follows:

$$\vec{E}(\vec{r}) = -j\omega \vec{A}(\vec{r}) - \nabla \varphi(\vec{r}) \tag{4}$$

where $\vec{A}$ is the magnetic vector potential and φ is the electric scalar potential, while f is the operating frequency where $\omega = 2\pi f$.

The first term in (4) is due to current flowing in the magnetotherapy device (coil), while the second one is due to accumulated free surface charges, represented by charge density ρ_s on the boundary S between regions with different material properties.

The electric scalar potential is governed by the Laplace equation

$$\Delta \varphi = 0 \tag{5}$$

everywhere except at the interfaces. The solution of (5) is integral of the following form:

$$\varphi(\vec{r}) = \int_S \frac{\rho_s(\vec{r}\,')}{4\pi\varepsilon_0} \frac{dS'}{R} \tag{6}$$

where $R = |\vec{r} - \vec{r}\,'|$ is the distance between the observation point $\vec{r}$ and the source point $\vec{r}\,'$.

Inserting (6) into (4), we obtain:

$$\vec{E}(\vec{r}) = -j\omega\vec{A}(\vec{r}) - \int_S \frac{\rho_s(\vec{r}\,')}{4\pi\varepsilon_0}\nabla\frac{1}{R}dS' \tag{7}$$

where ε_0 is the free space permittivity.

In case of singularity, where $R \to 0$, it is necessary to find the limiting values of the integral from (7), once when $\vec{r} \to \vec{r}\,'$ from the inside and the other time from the outside. In this limiting case, a small hemispherical region of radius ε needs to be excluded around the point on surface S. This region is denoted as S_ε, as depicted in Figure 2.

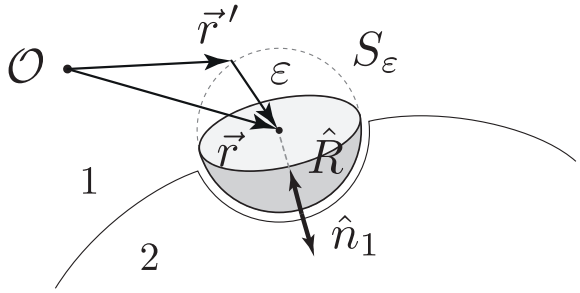

Figure 2. Treatment of singularity on the surface S [24].

The value of the surface integral (7) in the limiting case can be easily found [24]:

$$\lim_{R\to 0}\int_{S_\varepsilon}\frac{\rho_s(\vec{r}\,')}{4\pi\varepsilon_0}\nabla\frac{1}{R}dS' = \lim_{R\to 0}\frac{\rho_s(\vec{r}\,')}{4\pi\varepsilon_0}\int_{\theta=0}^{\pi/2}\int_{\varphi=0}^{2\pi}\left(-\frac{\vec{R}}{R^3}\right)\varepsilon^2\sin\theta\,d\theta\,d\varphi = -\frac{\rho_s(\vec{r}\,')}{2\varepsilon_0}(\hat{R}) \tag{8}$$

where $\hat{R} = -\hat{n}_1$ in region 1 and $\hat{R} = \hat{n}_1$ in surrounding region 2.

Using (8) and (7), the following expressions for the electric field are obtained in the vicinity of surface S, from the interior and the exterior side, respectively:

$$\vec{E}_{int}(\vec{r}) = -j\omega\vec{A}(\vec{r}) - \int_S \frac{\rho_s(\vec{r}\,')}{4\pi\varepsilon_0}\nabla\frac{1}{R}dS' - \hat{n}_1\frac{\rho_s(\vec{r}\,')}{2\varepsilon_0} \tag{9}$$

$$\vec{E}_{ext}(\vec{r}) = -j\omega\vec{A}(\vec{r}) - \int_S \frac{\rho_s(\vec{r}\,')}{4\pi\varepsilon_0}\nabla\frac{1}{R}dS' + \hat{n}_1\frac{\rho_s(\vec{r}\,')}{2\varepsilon_0} \tag{10}$$

By inserting (9) and (10) into boundary condition (2), followed by some additional steps, the following integral equation formulation can be obtained [25]:

$$\frac{\rho_s(\vec{r}\,')}{2\varepsilon_0} + \frac{\sigma_{int}-\sigma_{ext}}{\sigma_{int}+\sigma_{ext}}\int_S \frac{\rho_s(\vec{r}\,')}{4\pi\varepsilon_0}\nabla\frac{1}{R}dS' = \frac{\sigma_{ext}-\sigma_{int}}{\sigma_{int}+\sigma_{ext}}j\omega\vec{A}(\vec{r})\cdot\hat{n}_1; \quad \vec{r}\in S \tag{11}$$

The surface integral Equation (11) is written in terms of the unknown free surface charge density ρ_s on the surface S, hence it is sometimes called ρ-formulation. σ_{ext} in (11) denotes the known value of electrical conductivity σ_2, σ_3 or $\sigma_{air} = 0$, depending on the boundary.

After the surface charges ρ_s are determined, the eddy current density can be found using:

$$\vec{J}(\vec{r}) = \sigma_n\left[-j\omega\vec{A}(\vec{r}) - \nabla\varphi(\vec{r})\right] \tag{12}$$

where σ_n is the conductivity of the medium.

2.2. Excitation by Magnetotherapy Coil

Assuming a uniform current density I over a coil cross-section, the magnetic vector potential at observation point $\vec{r}$ can be determined from the integral [26]:

$$\vec{A}(\vec{r}) = \frac{\mu_0 MI}{4\pi} \oint_l \frac{\vec{dl}}{|\vec{r} - \vec{r}\,'|} \tag{13}$$

where μ_0 is the free space permeability, M is the number of coil windings, and $\vec{r}\,'$ is the position of the source point along the coil. The orientation of differential element $\vec{dl}$ along the coil is the same as the direction of coil current I. The magnetic vector potential (13) due to circular stimulating coil can be calculated easily if the coil is approximated by the N-sided polygon as follows:

$$\vec{A}(\vec{r}) = \frac{\mu_0 MI}{4\pi} \sum_{i=1}^{N} \frac{\Delta l_i}{R} \tag{14}$$

where Δl_i is the length of the polygon line segment, and R is the distance from observation to source point on the coil. The resultant magnetic vector potential at an arbitrary point in space can be determined by assembling the contributions from all linear segments.

The electric field due to stimulating coil can be found using:

$$\vec{E}(\vec{r}) = -j\omega\vec{A}(\vec{r}) \tag{15}$$

where ω is the angular frequency.

An illustrative example of the normalized electric field distribution in the plane below the circular coil and the so-called figure-of-eight coil can be seen in Figure 3.

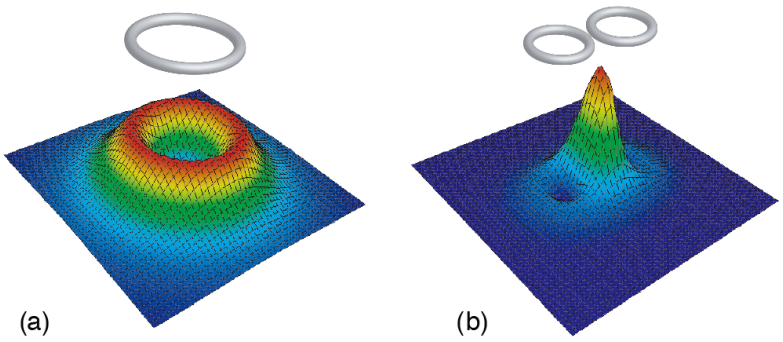

Figure 3. Normalized electric field above the circular coil (**a**) and the figure-of-eight coil (**b**). Adapted from [27].

As evidenced from Figure 3, in case of the circular coil, which is used traditionally in magnetotherapy, the maximum value of the electric field will be in the vicinity of coil windings, whereas in case of the figure-of-eight coil, this place is directly below the coil geometric center.

2.3. Numerical Solution

The numerical solution to integral Equation (11) was carried out via moments method (MoM). The boundary surface S of the human body is first discretized with triangular elements. The expansion of unknown surface charge density ρ_s is carried out using known basis function f_n:

$$\rho_s(\vec{r}) = \sum_{n=1}^{N} a_n f_n(\vec{r}) \tag{16}$$

with N denoting the number of triangles used to discretize the surface S and a_n the unknown coefficients to be solved for, respectively. The pulse basis functions, equal to

one for triangle T_n and zero elsewhere, have been utilized in the expansion, as depicted in Figure 4:

$$f_n(\vec{r}) = \begin{cases} 1 & ,\vec{r} \in T_n \\ 0 & ,\vec{r} \notin T_n \end{cases} \tag{17}$$

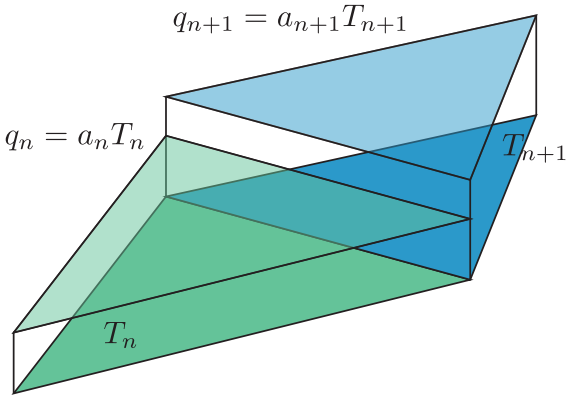

Figure 4. Illustration of piecewise-constant pulse basis function on triangles T_n and T_{n+1}. Electric charge on each triangle can be determined from charge density multiplied by triangle surface, denoted by T_n and T_{n+1}, respectively.

Inserting (17) into (16), the unknown surface charge density can be approximated. Multiplying Equation (11) with test functions $t_m(\vec{r})$, where $t_m(\vec{r}) = f_n(\vec{r})$, followed by integration over S, leads to the following system of N integral equations:

$$\sum_{n=1}^{N} a_n \int_S t_m(\vec{r}) \frac{\rho_s(\vec{r}\,')}{2\varepsilon_0} dS + \frac{\sigma_{int} - \sigma_{ext}}{\sigma_{int} + \sigma_{ext}} \sum_{n=1}^{N} a_n \int_S t_m(\vec{r}) \int_{S'} \frac{\rho_s(\vec{r}\,')}{4\pi\varepsilon_0} \nabla \frac{1}{R} dS'dS = \\ = \frac{\sigma_{ext} - \sigma_{int}}{\sigma_{int} + \sigma_{ext}} \sum_{n=1}^{N} a_n \int_S t_m(\vec{r}) j\omega \vec{A}(\vec{r}) \cdot \hat{n}_1 dS; \quad \vec{r} \in S \tag{18}$$

which can be recast in the following compact matrix form:

$$[\mathbf{Z}] \cdot \{\mathbf{I}\} = \{\mathbf{V}\} \tag{19}$$

The elements of the impedance matrix $\mathbf{Z}$ can be determined using:

$$Z_{mn} = \delta_{mn} \frac{T_m}{2\varepsilon_0} + \frac{\sigma_{int} - \sigma_{ext}}{\sigma_{int} + \sigma_{ext}} \int_{T_m} \int_{T_n} \frac{\hat{n}(\vec{r})}{4\pi\varepsilon_0} \nabla \frac{1}{R} dS'dS \tag{20}$$

while elements of the source vector $\mathbf{V}$ can be determined using the following:

$$V_m = \frac{\sigma_{ext} - \sigma_{int}}{\sigma_{int} + \sigma_{ext}} \int_{T_m} \hat{n}(\vec{r}) \cdot j\omega \vec{A}(\vec{r})\, dS \tag{21}$$

In (20), T_m and T_n denote the surfaces of observation and source triangles, respectively, while δ_{mn} represents the Kronecker delta (equal to 1 for $m = n$ and 0 otherwise).

The solution to the matrix Equation (19) is a a column vector $\mathbf{I}$ containing the unknown coefficients a_n. From these coefficients, the unknown surface charges can be found using (16), while the electric field can be found using expression (4).

Numerical solution to integrals (20) and (21) can be found elsewhere, e.g., in [28,29].

3. Human Body Model

3.1. Cylindrical Model

The typical position of the human body during the magnetotherapy procedure is depicted in Figure 5a.

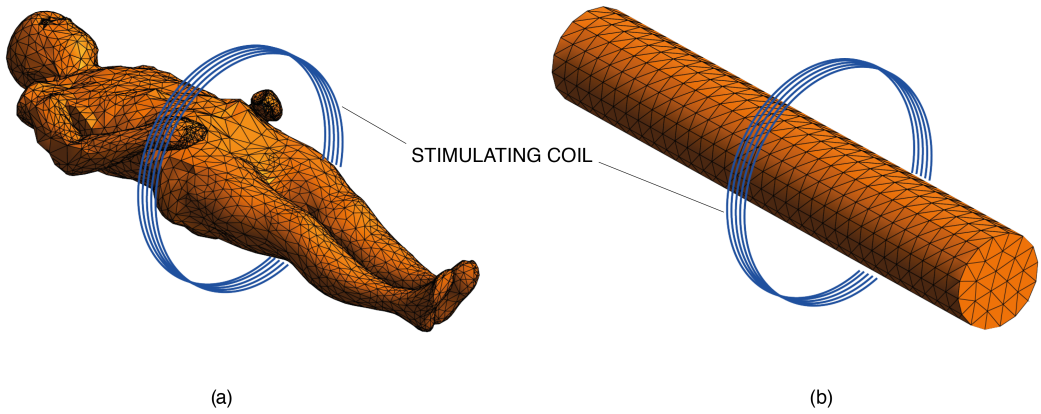

Figure 5. (**a**) Illustration of supine position during a magnetotherapy procedure. (**b**) Simple cylindrical human body model exposed to magnetic field of magnetotherapy device coil. The height of human body is 1.75 m, while diameter of cylindrical model is 0.3 m. Human body is modeled as having homogeneous conductivity $\sigma = 0.5$ S/m.

As a first approximation, the human body can be represented using a canonical geometry such as a parallelepiped [30,31] or a cylinder [31,32], as shown in Figure 5b.

The dimensions of the simplified cylindrical human body model are as follows: diameter $D = 30$ cm and height $h = 1.75$ m. Furthermore, the human body can be considered as having homogeneous properties, represented by the uniform value of electrical conductivity $\sigma = 0.5$ S/m.

It should be emphasized that the human body is of a geometrically complicated form whose composition is rather complex, consisting of various tissues with parameters that are often difficult to find. In addition to this, the electrical properties of tissues are dependent on the frequency, as depicted in Figure 6.

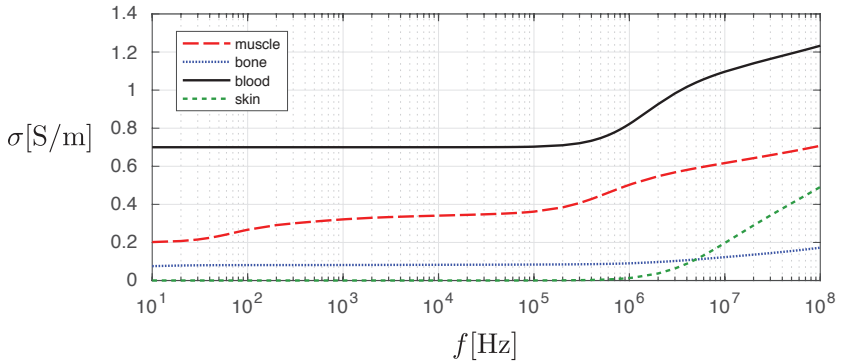

Figure 6. Frequency dependent electrical conductivity of several human body tissues and blood. Data from [33].

It should be noted that the numerical approach to magnetotherapy analysis presented in this work could be easily extended to include the anatomically realistic model of the human body, such as the one depicted in Figure 5a. The results presented in the following sections are obtained using a simplified cylindrical model.

3.2. Model Validation

The validation of the numerical model is carried out first. The results obtained using an approach based on integral equation Formulation (11), solved by MoM, is compared with the analytical approach. To this end, the disk model of human body [34] has been utilized. The human body exposed to ELF fields due to magnetotherapy device based on the analytical approach has been previously carried out in [17].

Assuming the exposure of human body to uniform magnetic flux density directed perpendicular to the human body, ($B = B_z$), the induced current density J_ϕ, circulating around the body axis, can be obtained using the following [17]:

$$|J_\phi| = \sigma \pi a f B_z \tag{22}$$

where homogeneous body with radius $a = 0.14$ m and height a is assumed, while body conductivity is $\sigma = 0.5$ S/m. Derivation of the analytical expression (22) can be found in Appendix A.

The analytical results for the induced current density obtained at several frequencies (f) of interest are given in Table 1.

Table 1. Comparison of induced current density due to magnetic field exposure at frequencies: f = 50, 75, and 100 Hz. Analytical results from [17], and numerical results obtained using proposed approach. Numerical results obtained at two points: 13.95 cm and 10 cm from the model axis.

	Analytical [17]			**Numerical, Point (13.95 cm)**			**Numerical, Point (10 cm)**		
B	**J [mA/m^2]**			**J [mA/m^2]**			**J [mA/m^2]**		
μT	f = 50 Hz	f = 75 Hz	f = 100 Hz	f = 50 Hz	f = 75 Hz	f = 100 Hz	f = 50 Hz	f = 75 Hz	f = 100 Hz
100	1.10	1.65	1.10	1.10	1.60	2.20	0.78	1.20	1.60
200	2.20	3.30	4.40	2.20	3.30	4.40	1.60	2.40	3.10
300	3.30	4.95	6.60	3.30	4.90	6.60	2.40	3.50	4.70
400	4.40	6.60	8.80	4.40	6.60	8.80	3.10	4.70	6.30
500	5.50	8.25	11.00	5.50	8.20	11.00	3.90	5.90	7.90

The results obtained using our numerical approach are also presented in Table 1. It is evident from Table 1 that excellent agreement between numerical and analytical approach is obtained at all three frequencies, thus validating the numerical approach. The only discrepancy found between the two approaches is in the scenario with $B = 100$ μT and $f = 100$ Hz, which can be attributed to a typographical error in [17].

The induced current density obtained obtained using our numerical approach is depicted in Figure 7.

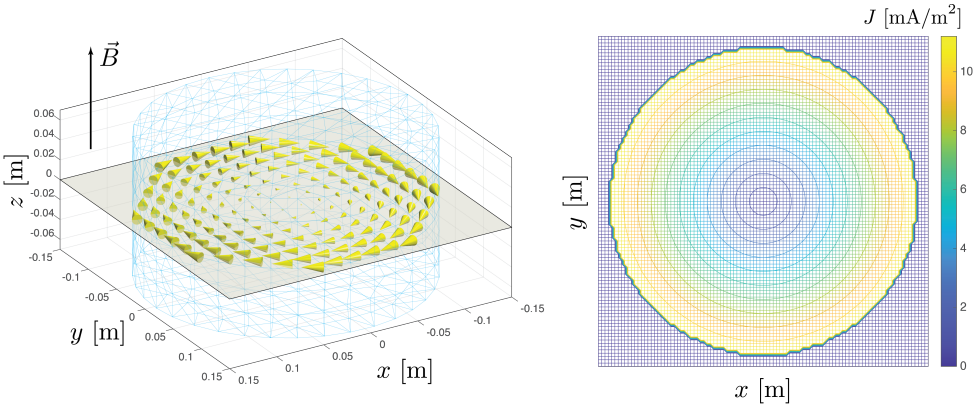

Figure 7. (**a**) Direction of the induced eddy current (yellow arrows) on the cross-section ($z = 0$) of homogeneous cylindrical model due to z-directed magnetic field B. (**b**) The induced eddy current values. The height of model is 0.14 m, while diameter of cylindrical model is 0.28 m. The conductivity σ = 0.5 S/m. $f = 100$ Hz and $B = 500$ μT.

The numerical results in Figure 7 are calculated in the x-y plane, i.e., in the transversal cross-section of homogeneous cylindrical model, at height $z = 0$. Note that the uniform magnetic field oriented in z direction will induce the circular current loops in the x-y plane. The value of the induced current density increases linearly as the axial distance increases, as shown in Figure 7b and Table 1, for two points (r = 10 cm and $r \approx 14$ cm).

4. Numerical Results and Discussion

The following sections presents some illustrative results of the magnetotherapy coil induced current density and the induced electric field obtained using the proposed numerical approach. The simplified human body model is utilized. The analyses of several magnetotherapy coil parameters as well as body conductivity are carried out to determine their effect on the induced current density and the induced electric field.

4.1. Parameter Analysis of Stimulating Coil

The first set of results are related to the magnetotherapy coil parameter analysis, such as the number of windings N, the coil diameter r, and the coil length L, as illustrated in Figure 8.

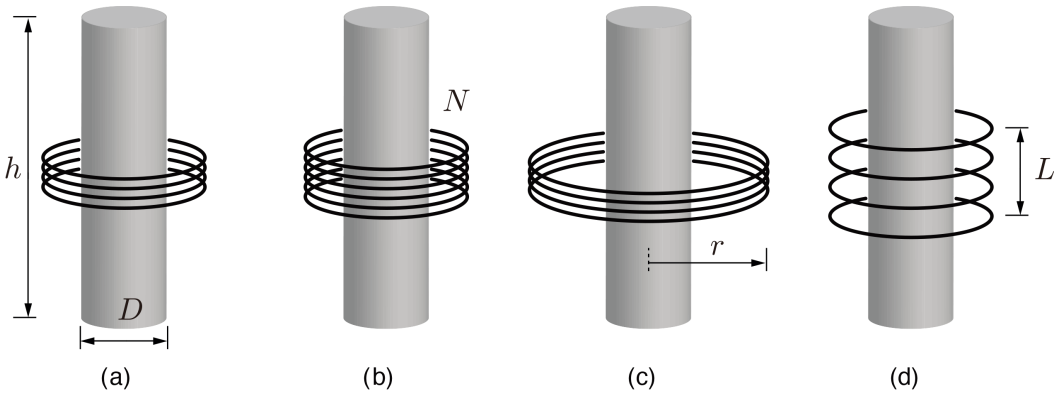

Figure 8. Analysis of coil parameters: (**a**) default configuration, (**b**) effect of coil windings N, (**c**) effect of coil radius r, and (**d**) effect of coil length L.

The numerical results are reported in Figure 9 and Tables 2 and 3.

4.1.1. Number of Coil Windings

The first set of results are related to varying number of coil windings. The default coil parameters are as follows: coil radius r = 0.3 m, coil length L = 0.4 m, coil current I = 1 A, and frequency f = 10 kHz. The coil is positioned coaxially with respect to human body, as depicted in Figure 8b. The geometrical center of the body ($z = 0$) corresponds to the center of the coil.

Magnetic coils of varying number of turns $N = [3, 4, 5, 6]$ have been considered, with the results presented in Table 2.

Table 2. The effect of number of coil windings N.

Coil Windings N	J [mA/m^2]	E [V/m]
3	10.1	0.0202
4	14.2	0.0284
5	18.2	0.0364
6	22.3	0.0446

Due to symmetry of the problem (the coil is concentric with regard to the body), the results given in Table 2 were obtained 1 cm from the model surface directly under the coil windings. Table 2 shows the linear dependence of both induced current density and induced electric field on the number of magnetotherapy coil windings. Doubling the coil

windings (from 3 to 6), the values of both induced current density and induced electric field will roughly double. However, more importantly, for each coil turn the induced current density will increase by additional 4.1 mA/m^2.

4.1.2. Magnetotherapy Coil Radius

The following results are obtained using the coil of length L = 0.1 m, with N = 4 turns, f = 10 kHz, with varying coil radii, r = [0.175, 0.2, 0.25, 0.3] m. The axial distribution of the induced current density (depth 1 cm from the surface) is depicted in Figure 9.

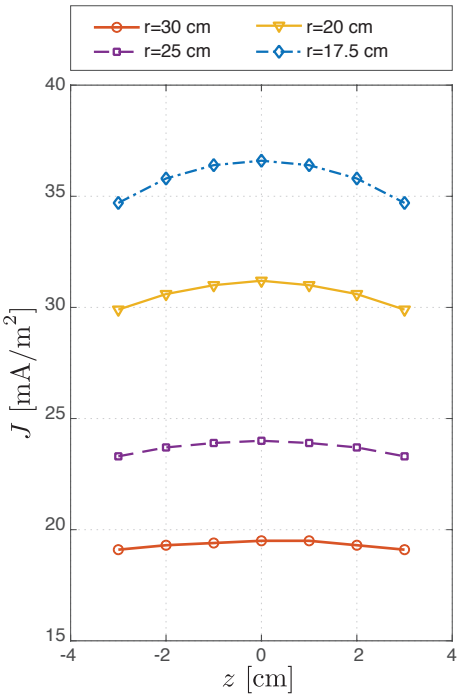

Figure 9. Axial distribution of induced current density directly under coil geometric center. Current density J [mA/m^2] calculated at points 1 cm under the cylinder surface. Coil radii: r = [17.5, 20, 25, 30] cm.

As seen from Figure 9, an approximate shape of a parabola is obtained. In all cases, the highest values of induced current density are at the point directly under the coil center (z = 0). The highest values of induced current density are achieved with smallest diameter coil as the coil is located closer to the body.

The results show that the gradient of the induced current density with decreasing coil radius will be more pronounced directly under the coil center. For example, when decreasing coil radius from 30 cm to 25 cm, the induced current will increase by 4.5 mA/m^2 at z = 0 compared to 4.2 mA/m^2 at the location 3 cm along the axial direction (z = 3 cm).

4.1.3. Coil Length

The next results are obtained for magnetotherapy coils of various lengths L, ranging from 10 cm to 40 cm, while other parameters were similar to previous calculations. The results for the induced fields are given in Table 3.

The results from Table 3 show approximately linear dependence. The shorter the length of the coil L, the higher the values of induced current density J and induced electric field E.

Table 3. The effect of coil length L.

Coil Length L [cm]	J [mA/m^2]	E [V/m]
10	19.5	0.039
20	17.9	0.0358
30	16.0	0.032
40	14.2	0.0284

4.2. Human Body Model Parameter Analysis

The second set of results are related to the parameter analysis of the utilized simple human body model, i.e., the cylinder height h, the diameter D, and the electrical conductivity σ, as illustrated in Figure 10.

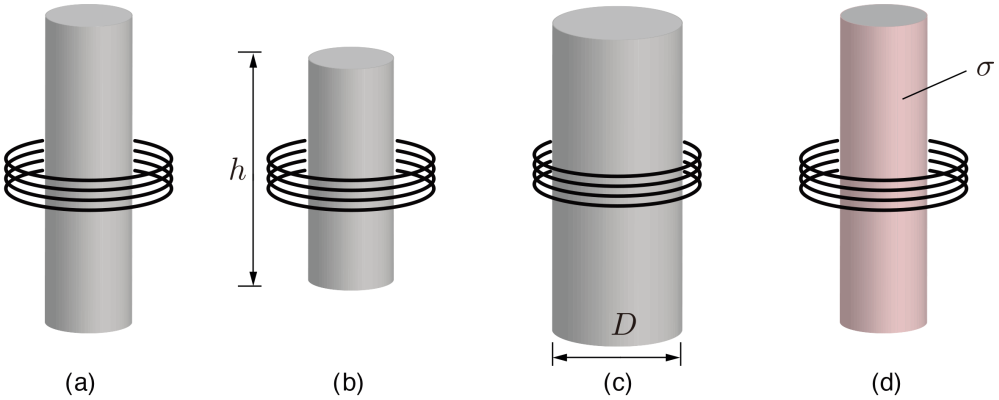

Figure 10. Analysis of model parameters: (**a**) default configuration, (**b**) effect of model height h, (**c**) effect of model diameter D, and (**d**) effect of body conductivity σ.

4.2.1. Effect of Model Height

The height h of the human model is varied first. The results obtained using the following values of $h = [1.55, 1.65, 1.75, 1.85, 1.95]$ m, are depicted in Figure 11.

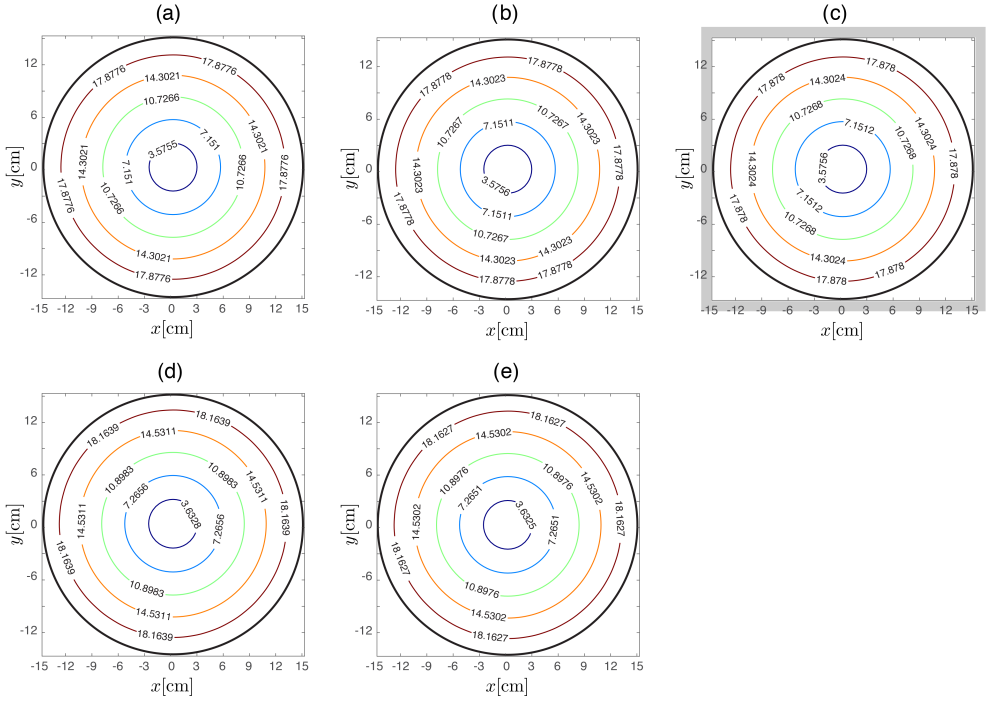

Figure 11. The effect of model height h: (**a**) 1.55 m, (**b**) 1.65 m, (**c**) 1.75 m, (**d**) 1.85 m, and (**e**) 1.95 m. Iso-contours of the induced current density in the x-y cross-section at $z = 0$. Boxed results denote the default model height.

The selected values of body height are related to the standing height percentiles for male and female Caucasian adult persons from nine countries studied in [35].

The results for the induced current density depicted in Figure 11 are obtained at the transversal cross-section ($x - y$ plane) with $z = 0$. The initial coil settings were utilized, with concentric position of the stimulating coil, as depicted in Figure 10b.

As seen from Figure 11, very similar distribution of the induced current density is obtained in all models. In two higher models (h = 1.85 m and h = 1.95 m), around a 2% higher value is obtained compared to the default model (h = 1.75 m), which can be attributed to the induced surface charges on the top and bottom base moved further from the coil central position. However, if this was the only reason, then the values of the induced current density in two smaller models h = 1.55 m and h = 1.65 m should have been lower than the default model, which was not the case. Another possible explanation for the different values could be attributed to the number of triangular elements used to discretize the model surface. Further analysis should be carried out to determine whether this is the possible reason; however, this is outside the scope of this work.

4.2.2. Effect of Model Thickness

The following results are obtained using body models of varying thickness. We considered different values of body diameter $D = [25, 30, 35, 40, 45]$ cm. The default magnetotherapy coil, positioned centrally to the model, was considered. The results are depicted in Figure 12.

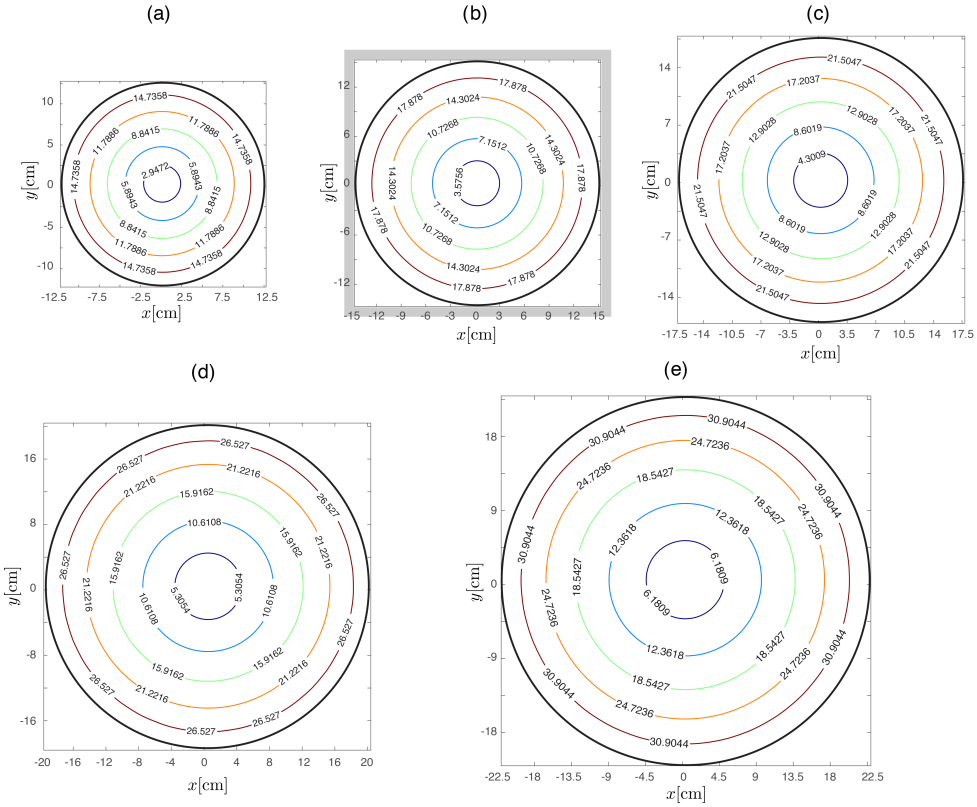

Figure 12. The effect of model diameter h: (**a**) 25 cm, (**b**) 30 cm, (**c**) 35 cm, (**d**) 40 cm, and (**e**) 45 cm. Iso-contours of the induced current density in the x-y cross-section at $z = 0$. Boxed results denote the default model height.

As is evident from Figure 12, using the model with larger diameter D positioned within the same stimulating coil has the effect of body being closer to the coil windings. As a result, the higher values of the induced current density are obtained. The relative increase in the induced current density 2 cm from the body surface (the first iso-contours

from Figure 12) is 16%, 32%, and 40% for the three models with a larger diameter. In case of smaller diameter model, the relative decrease with respect to default body model is around 20%. The results suggest that, depending on the human body size, in order to obtain the similar value of induced current density, the appropriate size of the stimulating coil should be utilized. Of course, there are other ways to compensate for this such as decreasing the coil current.

4.2.3. Effect of Body Conductivity

The final results obtained for the coaxial position of magnetic coil are related to different conductivity values of homogeneous model, as given in Table 4. The results were obtained at a depth of 1 cm directly under the coil center. The following coil parameters were used: r = 0.3 m, L = 0.4 m, I = 1 A, and N = 4 turns.

Table 4. The results using different biological body conductivity σ.

Conductivity σ [S/m]	J [mA/m^2]	E [V/m]
0.3	8.5	0.02833
0.4	11.4	0.0285
0.5	14.2	0.0284
0.6	17.0	0.02833

As expected, the results from Table 4 show that induced current density increases proportionally with increasing conductivity. However, the value of the induced electric field remains constant in all calculations because $J = \sigma \cdot E$.

It should be emphasized that using the homogeneous body conductivity is a great simplification as the human body consists of many tissues with different parameter values. Moreover, there are many uncertainties regarding the exact value of particular tissue parameter, particularly at lower frequencies [36,37]. The uncertainty of the tissue electrical conductivity can be taken into account via statistical approaches such as the polynomial chaos method (PCM) or the stochastic collocation method (SCM). An interested reader could find more details on several examples of the SCM approach applied to modeling biomedical applications including transcranial electrical stimulation (TES) [38] and transcranial magnetic stimulation (TMS) [39].

4.3. Displacement of Magnetotherapy Coil

The final set of results obtained using cylindrical model are related to magnetotherapy coil positioned perpendicular to body model, as depicted in Figure 13.

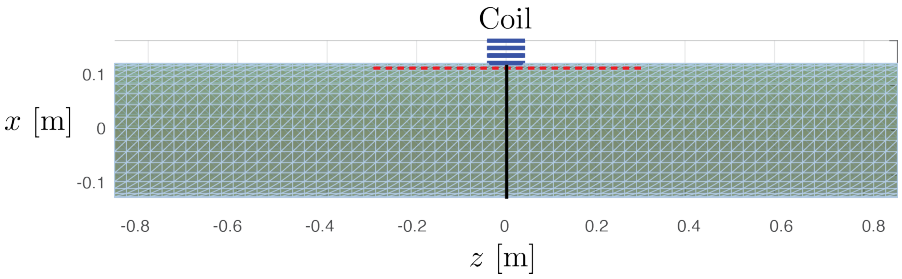

Figure 13. Perpendicular orientation of coil with regard to the human body. The red dashed line denotes observation points 1 cm under the cylinder surface (axial distribution $z = [-30, +30]$ cm), while the full black line (z = 0) denotes the cross-section plane where induced current density is also calculated.

The coil is placed at a 1 mm distance from the body, with coil axis perpendicular to the human body axis. The observation points are along the z-axis of the model at 1 cm from the body surface. The default parameters of the human body model are used: h = 1.75 m, D = 30 cm, and σ = 0.5 S/m.The results are obtained with following coil

parameters: L = 5 cm; r = 3.75 cm, N = 4 turns, I = 1 A, and f = 10 kHz. The results are presented in Figures 14–16.

The induced current density along the body axis is shown in Figure 14.

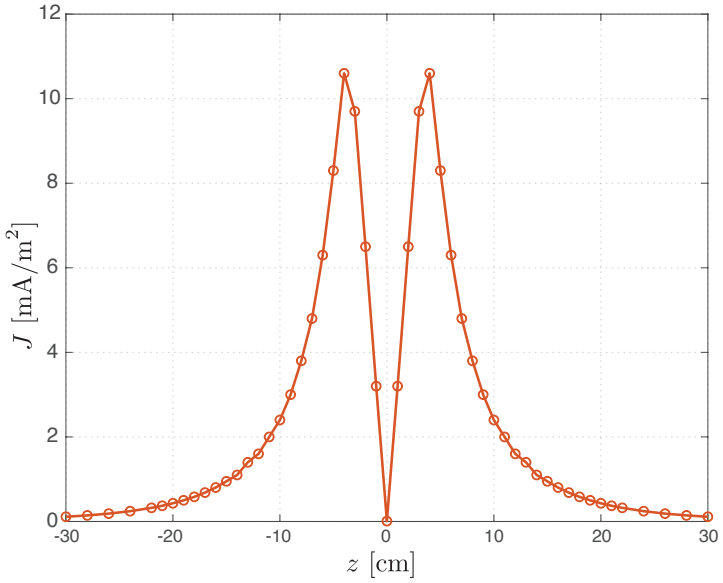

Figure 14. Axial distribution of induced current density directly under coil geometric center. Current density J [mA/m^2] calculated at points 1 cm under the cylinder surface.

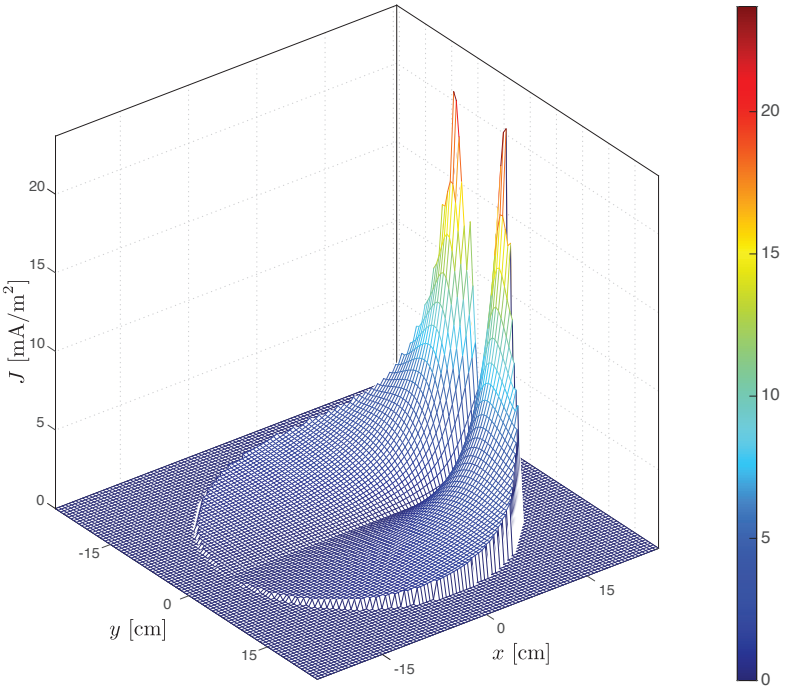

Figure 15. Induced current density J [mA/m^2] at the cross-section z = 0 of cylindrical body. The coil (not shown) center located at x = 15 cm and y = 0 cm.

The results from Figure 14 indicate that at the body center ($z = 0$), while the induced current density and the induced electric field are approximately 0. Moving away from the center along the z-axis (in both directions), these values increase until z = 4 cm (and $z = -4$ cm), corresponding to position directly under the coil windings where the induced current density reaches 10.6 mA/m^2, and the induced electric field reaches a correspond-

ing value of 0.0212 V/m. With the increasing distance, both J and E begin to decline exponentially.

The results for the induced current density obtained at the horizontal cross-section ($z = 0$), corresponding to coil axis, are shown in Figure 15.

As is evident from Figure 15, the induced current density along the coil axis is basically nonexistent when the coil is oriented perpendicular with respect to the body. Moreover, a very sharp decline in the induced current density can be noticed, when moving from the model surface. These results indicate that, when using the circular magnetotherapy coil, the highest value of the induced field will be obtained very close to coil windings. Thus, if the ultimate goal is to achieve high values of induced field in a very focused region, a very different coil geometry, such as figure-of-eight, should be considered.

The final numerical results, obtained in x-y cross-section of cylindrical model, at $z = 0$, are depicted in Figure 16.

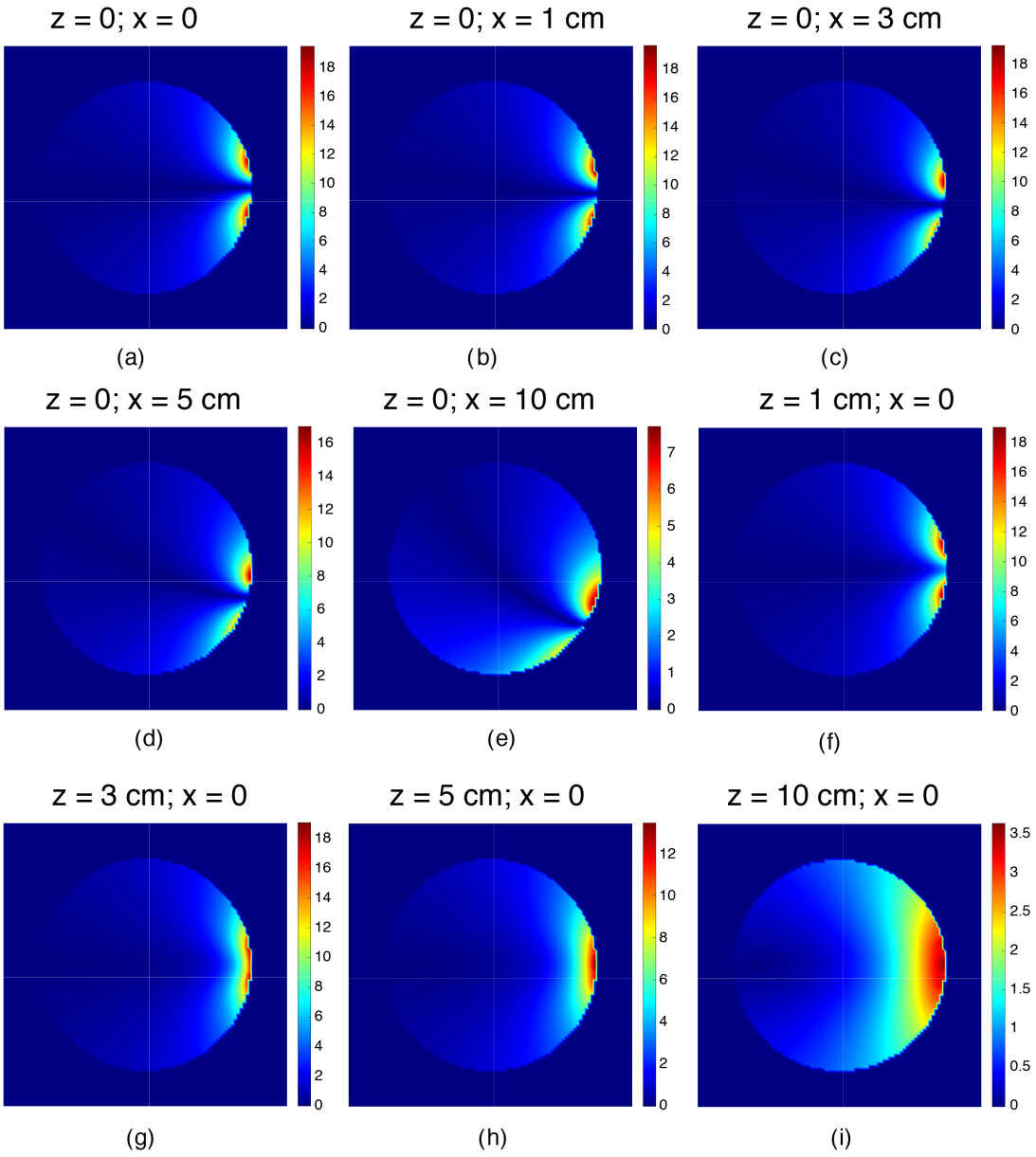

Figure 16. Distribution of induced current density on the cross-section of model. (**a**) The initial position of coil geometrical center ($z = 0$ and $x = 0$). The displacement along the x-axis: (**b**–**e**). The displacement along z-axis (body height): (**f**–**i**). All values in [mA/m^2].

The results shown in Figure 16 illustrate the effect of the perpendicularly oriented coil displacement on the induced current density. The initial position of the coil is with its center at $x = 0, z = 0$, as shown in Figure 14. The coil is displaced with respect to x and z directions by 1 cm, 3 cm, 5 cm, and 10 cm.

As evident from Figure 16b–e, horizontal displacement of coil along x-axis, results in the position with maximum induced current density also being shifted. As already mentioned, the maximum induced value will be under the coil windings. At the point 1 cm below the surface, the obtained induced current density is 4.2 $\mu A/m^2$, 11.2 $\mu A/m^2$, 10.5 $\mu A/m^2$, and 3.5 $\mu A/m^2$ when the coil is moved 1 cm, 3 cm, 5 cm, and 10 cm, respectively.

Compared to this, the vertical displacement of coil along z-axis, as shown in Figure 16f–i, will result in similar values of J at the same point; however, a different distribution of induced current density will be obtained. The coil displacement by 1 cm, 3 cm, 5 cm, and 10 cm, respectively, will result in the corresponding induced current density of 4 $\mu A/m^2$, 10.7 $\mu A/m^2$, 10.1 $\mu A/m^2$, and 3.3 $\mu A/m^2$ at the point 1 cm from the surface. However, in this case, a maximum value of the induced current will be spread over a considerably larger cross-sectional area, i.e., a smoother gradient of the induced current density will be achieved.

5. Conclusions

This paper presented the numerical model for a magnetotherapy device based on the surface integral equation formulation. The numerical solution was carried out using a method of moments technique. The illustrative numerical results for the induced current density and the induced electric field were obtained using a simplified geometry for the human body. The analyses of several magnetotherapy device parameters were carried out, as well as for different values of homogeneous body conductivity, in order to assess their effects on the parameters of interest. The presented numerical approach could easily be extended to more complicated body geometries. Future works will thus be related to tackling an anatomically realistic model of the human body using the proposed approach.

Author Contributions: Conceptualization, methodology, writing—original draft preparation, and supervision: M.C.; formal analysis and investigation: B.S.; writing—review and editing and visualization: M.C. and B.S. All authors have read and agreed to the published version of the manuscript.

Funding: This research received no external funding.

Data Availability Statement: The data presented in this study are available on request from the corresponding author.

Conflicts of Interest: The authors declare no conflicts of interest.

Abbreviations

The following abbreviations are used in this manuscript:

ELF	extremely low-frequency
EMF	electromagnetic field
PEMF	pulsed electromagnetic field
TMS	transcranial magnetic stimulation
SCS	spinal cord stimulation
MOM	method of moments
PCM	polynomial chaos method
SCM	stochastic collocation method
TES	transcranial electrical stimulation

Appendix A

The analytical expression for the induced circular current density due to the normally oriented magnetic flux density can be assessed using the disk human body model, as shown in Figure A1.

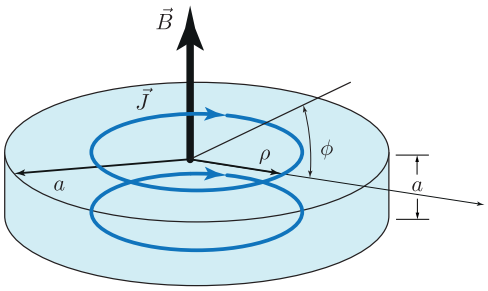

Figure A1. Disk model of the human body [24].

This analytical model has been proposed in [34] to provide rapid estimation of the ELF magnetic field exposure. The disk is assumed to be homogeneous with conductivity σ and radius a. The analytical expression for the current density can be derived using the differential form of Faraday's law, which for the time harmonic fields is given by:

$$\nabla \times \vec{E} = -j\omega\vec{B} \tag{A1}$$

where $\vec{E}$ is the impressed electric field, which is related to the induced current density via:

$$\vec{J} = \sigma\vec{E} \tag{A2}$$

Combining (A1) and (A2), followed by integration over an arbitrary surface S, results in the following:

$$\int_S \nabla \times \vec{J}\, d\vec{S} = -\int_S j\sigma\omega\vec{B}\, d\vec{S} \tag{A3}$$

Using the Stokes' theorem, the left hand side of (A3) can be rewritten as a line integral over curve c bounding the surface S:

$$\oint_c \vec{J}\, d\vec{s} = -j\omega\sigma\vec{B}\int_S d\vec{S} \tag{A4}$$

The expression (A4) can be expanded in the cylindrical coordinates as:

$$\int_0^{2\pi} J_\phi \rho\, d\phi = -j\omega\sigma B_z \int_0^{\rho'}\int_0^{2\pi} \rho\, d\rho\, d\phi \tag{A5}$$

where ω is the angular frequency.

Taking into account the rotational symmetry, the integration results in:

$$J_\phi \cdot 2\pi\rho = -j\omega\sigma B_z \rho^2 \pi \tag{A6}$$

Substituting $\omega = 2\pi f$ in (A6), the following expression for the induced current density inside the human disk model is obtained:

$$\left|J_\phi\right| = \sigma\pi\rho f \cdot B_z \tag{A7}$$

From the current density, the total current flowing through the cross-section of the disk, can be simply calculated:

$$I = \int_S \vec{J}\, d\vec{S} = \int_0^a\int_0^{2\pi} \sigma\pi f B_z \rho\, d\rho\, dz = \sigma\pi f B_z \int_0^a\int_0^{2\pi} \rho\, d\rho\, dz = \sigma\pi f B_z \frac{a^3}{2} \tag{A8}$$

References

1. Markov, M.S. Pulsed electromagnetic field therapy history, state of the art and future. *Environmentalist* **2007**, *27*, 465–475. [CrossRef]
2. Bassett, C.; Pawluk, R.; Pilla, A. Acceleration of fracture repair by electromagnetic fields. A surgically noninvasive method. *Ann. N. Y. Acad. Sci.* **1974**, *238*, 242–262. [CrossRef]
3. Kuipers, N.T.; Sauder, C.L.; Ray, C.A. Influence of static magnetic fields on pain perception and sympathetic nerve activity in humans. *J. Appl. Physiol.* **2007**, *102*, 1410–1415. [CrossRef] [PubMed]
4. Yu, S.; Shang, P. A review of bioeffects of static magnetic field on rodent models. *Prog. Biophys. Mol. Biol.* **2014**, *114*, 14–24. [CrossRef] [PubMed]
5. Basford, J.R. A historical perspective of the popular use of electric and magnetic therapy. *Arch. Phys. Med. Rehabil.* **2001**, *82*, 1261–1269. [CrossRef] [PubMed]
6. Brown, C.S.; Ling, F.W.; Wan, J.Y.; Pilla, A.A. Efficacy of static magnetic field therapy in chronic pelvic pain: A double-blind pilot study. *Am. J. Obstet. Gynecol.* **2002**, *187*, 1581–1587. [CrossRef] [PubMed]
7. Carter, R.; Hall, T.; Aspy, C.B.; Mold, J. The effectiveness of magnet therapy for treatment of wrist pain attributed to carpal tunnel syndrome. *J. Fam. Pract.* **2002**, *51*, 38–40. [PubMed]
8. Richmond, S.J. Magnet therapy for the relief of pain and inflammation in rheumatoid arthritis (CAMBRA): A randomised placebo-controlled crossover trial. *Trials* **2008**, *9*, 1–17. [CrossRef] [PubMed]
9. Flamm, B. Magnet therapy: Extraordinary claims, but no proved benefits. *Br. Med. J.* **2006**, *332*, 4.
10. Pipitone, N.; Scott, D.L. Magnetic pulse treatment for knee osteoarthritis: A randomised, double-blind, placebo-controlled study. *Curr. Med. Res. Opin.* **2001**, *17*, 190–196. [CrossRef]
11. Kessler, T.M.; Mordasini, L.; Weisstanner, C.; Jüni, P.; da Costa, B.R.; Wiest, R.; Thalmann, G.N. Sono-electro-magnetic therapy for treating chronic pelvic pain syndrome in men: A randomized, placebo-controlled, double-blind trial. *PLoS ONE* **2014**, *9*, e113368. [CrossRef]
12. Galovic, P.; Celan, D.; Hernja-Rumpf, T. Short term effect of PEMF magnetotherapy on chronic Low back pain. *J. Magn.* **2018**, *23*, 553–558. [CrossRef]
13. Sengupta, S.; Balla, V.K. A review on the use of magnetic fields and ultrasound for non-invasive cancer treatment. *J. Adv. Res.* **2018**, *14*, 97–111. [CrossRef] [PubMed]
14. Paolucci, T.; Pezzi, L.; Centra, A.M.; Giannandrea, N.; Bellomo, R.G.; Saggini, R. Electromagnetic field therapy: A rehabilitative perspective in the management of musculoskeletal pain—A systematic review. *J. Pain Res.* **2020**, *13*, 1385–1400. [CrossRef] [PubMed]
15. Hallett, M. Transcranial magnetic stimulation: A primer. *Neuron* **2007**, *55*, 187–199. [CrossRef] [PubMed]
16. Oakley, J.C.; Prager, J.P. Spinal cord stimulation: Mechanisms of action. *Spine* **2002**, *27*, 2574–2583. [CrossRef] [PubMed]
17. Poljak, D.; Sesnic, S.; Cavka, D.; Titlic, M.; Mihalj, M. The human body exposed to a magnetotherapy device magnetic field. *WIT Trans. Biomed. Health* **2009**, *13*, 203–211.
18. Miaskowski, A.; Krawczyk, A.; Ishihara, Y. Computer modelling of magnetotherapy in orthopedic treatments. *COMPEL Int. J. Comput. Math. Electr. Electron. Eng.* **2010**, *24*, 1015–1021. [CrossRef]
19. Krawczyk, A.; Miaskowski, A.; Łada-Tondyra, E.; Ishihara, Y. Healing of Orthopaedic Diseases by Means of Electromagnetic Field. *Acta Tech. Jaurinensis* **2011**, *4*, 357–364.
20. Cieśla, A.; Kraszewski, W.; Tadeusiewicz, R. Visualization of magnetic field generated by portable coil designed for magnetotherapy. *Przegled Elektrotechniczny* **2012**, *88*, 127–131.
21. Richter, A.; Ferková, Ž. Physical and energy analysis of therapy applying low-dynamic magnetic fields. In Proceedings of the 2017 IEEE International Workshop of Electronics, Control, Measurement, Signals and Their Application to Mechatronics (ECMSM), Donostia, Spain, 24–26 May 2017; pp. 1–5.
22. Syrek, P. Uncertainty problem as illustrated by magnetotherapy. *Appl. Comput. Electromagn. Soc. J.* **2019**, *34*, 1445–1452.
23. Cvetković, M.; Sučić, B. Magnetotherapy Device Induced Fields in Simplified Human Body Model. In Proceedings of the 2023 8th International Conference on Smart and Sustainable Technologies (SpliTech), Split/Bol, Croatia, 20–23 June 2023; pp. 1–6. [CrossRef]
24. Poljak, D.; Cvetkovic, M. *Human Interaction with Electromagnetic Fields: Computational Models in Dosimetry*; Academic Press: Cambridge, MA, USA, 2019.
25. Makarov, S.N.; Noetscher, G.M.; Nazarian, A. *Low-Frequency Electromagnetic Modeling for Electrical and Biological Systems Using MATLAB*; John Wiley & Sons: Hoboken, NJ, USA, 2015.
26. Cvetković, M.; Poljak, D.; Haueisen, J. Analysis of Transcranial Magnetic Stimulation Based on the Surface Integral Equation Formulation. *Biomed. Eng. IEEE Trans.* **2015**, *62*, 1535–1545. [CrossRef] [PubMed]
27. Luquet, S.; Barra, V.; Lemaire, J.J. Transcranial magnetic stimulation: Magnetic field computation in empty free space. In Proceedings of the 2005 IEEE Engineering in Medicine and Biology 27th Annual Conference, Shanghai, China, 17–18 January 2006; pp. 4365–4368.
28. Dodig, H.; Cvetković, M.; Poljak, D. On the Computation of Singular Integrals Over Triangular Surfaces in R3. *WIT Trans. Eng. Sci.* **2019**, *122*, 95.

29. Cvetković, M.; Lojić Kapetanović, A.; Poljak, D.; Dodig, H. On the Applicability of Numerical Quadrature for Double Surface Integrals at 5G Frequencies. *J. Commun. Softw. Syst.* **2022**, *18*, 42–53. [CrossRef]
30. Kuster, N.; Balzano, Q. Energy absorption mechanism by biological bodies in the near field of dipole antennas above 300 MHz. *IEEE Trans. Veh. Technol.* **1992**, *41*, 17–23. [CrossRef]
31. Rasic, P.; Skiljo, M.; Blazevic, Z.; Doric, V.; Poljak, D. Simulation of human body exposure to high and low frequency wireless power transfer systems using simplified models. In Proceedings of the 2018 3rd International Conference on Smart and Sustainable Technologies (SpliTech), Split, Croatia, 26–29 June 2018; pp. 1–6.
32. King, R.W.; Sandler, S.S. Electric fields and currents induced in organs of the human body when exposed to ELF and VLF electromagnetic fields. *Radio Sci.* **1996**, *31*, 1153–1167. [CrossRef]
33. Hasgall, P.; Di Gennaro, F.; Baumgartner, C.; Neufeld, E.; Lloyd, B.; Gosselin, M.C.; Payne, D.; Klingenböck, A.; Kuster, N. IT'IS Database for Thermal and Electromagnetic Parameters of Biological Tissues, Version 4.1, 22 February 2022. Available online: https://itis.swiss/database (accessed on 17 February 2024).
34. *IEC 62226-2-1:2004*; Exposure to Electric or Magnetic Fields in the Low and Intermediate Frequency Range—Methods for Calculating the Current Density and Internal Electric Field Induced in the Human Body—Part 2-1: Exposure to Magnetic Fields—2D Models. IEC: Geneva, Switzerland, 2004; pp. 1–113.
35. Cassola, V.; Milian, F.; Kramer, R.; de Oliveira Lira, C.; Khoury, H. Standing adult human phantoms based on 10th, 50th and 90th mass and height percentiles of male and female Caucasian populations. *Phys. Med. Biol.* **2011**, *56*, 3749. [CrossRef] [PubMed]
36. Gabriel, C.; Peyman, A.; Grant, E.H. Electrical conductivity of tissue at frequencies below 1 MHz. *Phys. Med. Biol.* **2009**, *54*, 4863. [CrossRef] [PubMed]
37. De Santis, V.; Chen, X.L.; Laakso, I.; Hirata, A. An equivalent skin conductivity model for low-frequency magnetic field dosimetry. *Biomed. Phys. Eng. Express* **2015**, *1*, 015201. [CrossRef]
38. Šušnjara, A.; Verhnjak, O.; Poljak, D.; Cvetković, M.; Ravnik, J. Uncertainty quantification and sensitivity analysis of transcranial electric stimulation for 9-subdomain human head model. *Eng. Anal. Bound. Elem.* **2022**, *135*, 1–11. [CrossRef]
39. Cvetković, M.; Šušnjara, A.; Poljak, D. Deterministic–stochastic modeling of transcranial magnetic stimulation featuring the use of method of moments and stochastic collocation. *Eng. Anal. Bound. Elem.* **2023**, *150*, 662–671. [CrossRef]